Title
A NEW APPROACH TO CHARACTERIZING FLOW IN SINGLE FRACTURES

Authors
Muralidhar, K.
Long, J.C.S.

Publication Date
1987-04-01

LBL-22114 c.2

Lawrence Berkeley Laboratory
UNIVERSITY OF CALIFORNIA

EARTH SCIENCES DIVISION

To be published as a chapter in
Flow and Transport through Unsaturated Fractured Rock, D. Evans and J. Nicholson, Eds.,
American Geophysical Union, Washingtion, DC

A NEW APPROACH TO CHARACTERIZING FLOW IN SINGLE FRACTURES

K. Muralidhar and J.C.S. Long

April 1987

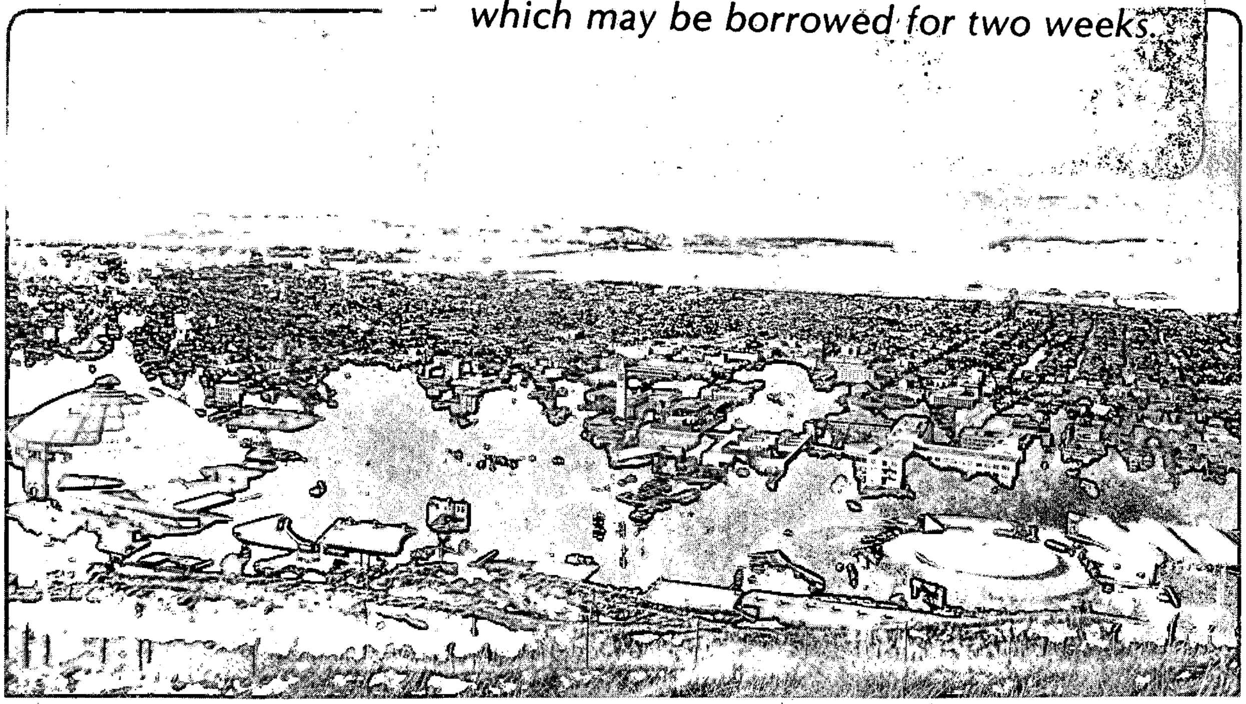

LBL-22114 c.2

Prepared for the U.S. Department of Energy under Contract DE-AC03-76SF00098

DISCLAIMER

A NEW APPROACH TO CHARACTERIZING FLOW IN SINGLE FRACTURES

K. Muralidhar and J. C. S. Long

Earth Sciences Division, Lawrence Berkeley Laboratory
University of California, Berkeley, California 94720

Abstract. A numerical method which determines fluid movement in a single fracture is described in the present study. This method allows for variable fracture aperture and the presence of contact areas which impose tortuosity on the flow. The objective behind developing such a technique is to investigate the way in which geometry controls fluid motion. Given the change in fracture geometry due to changes in stress, this technique can be used to determine the hydrologic properties of a fracture. The fluid behavior is described by the Navier-Stokes' equations. Hence, the validity of constitutive relationships between flux and gradient, such as cubic law can be examined.

Introduction

Current practice in modeling fluid flow in single rock fractures is to assume that each fracture can be treated as a channel whose walls are parallel planar plates. Recent laboratory and field experience has clearly demonstrated that flow in fractures that are subject to stress and infilling may occur in channels within the fracture. The present work describes a numerical method which can be used to investigate how fluid motion is determined by void geometry. The problem of characterizing flow in fractures has two parts. The first part concerns identification of the geometry of the conduits. The second part involves solving the flow problem in a prescribed geometry.

Determination of void geometry is not easy. Some approaches include taking profiles on each of the bounding surfaces and using variograms of these profiles to simulate the topography on a grid. The void geometry is given by the distances between the two surfaces and the change in the geometry in response to externally applied stress can be calculated [Hopkins et al., 1987]. Pyrak-Nolte et al. [1987] describe an alternative approach which involves filling fractures with low melting-point metal allowing the metal to cool, separating the fracture and photographing each side, thus revealing a pattern of the distribution of contact areas.

In the present work, we concentrate on the calculation of flow in a complex geometry, once the geometry is specified.

Conventional analyses assume that Darcy's law is valid for flow in a fracture, as it is for a homogeneous porous medium that is, flux is proportional to pressure gradient. The equivalent permeability of the fracture is usually derived from the "cubic law", which governs fully developed laminar flow through parallel plates. As an alternative, Tsang [1984] proposed a method using the analogy of an electrical resistance network. In the present study, none of these simplifications is employed and the governing flow equations are derived from Newton's second law of motion. These are the Navier-Stokes' equations [Schlichting, 1979], which determine flow for a prescribed pressure drop and hence the permeability of the rock fracture. Since these equations are non-linear, it can be expected that the amount of flow will not necessarily be linearly related to the pressure drop. Thus a fracture may not have a unique permeability. In this work, the flow is taken as steady, laminar and incompressible. The numerical scheme is general enough to be applicable to both two and three dimensional problems. Specific examples of flow calculation are discussed in this paper.

There are two principal difficulties in solving the Navier-Stokes equations for flow in a fracture. The first of these is the determination of pressure from the constraint of incompressibility. To allow for second order approximation of the pressure field, a Poisson equation of pressure has been used in the present study. The second difficulty arises from the complex flow geometry, on which the boundary conditions have to be specified. This has been dealt with using a grid transformation technique which maps the complex flow domain into a simple one. This procedure builds the details of the flow boundaries into the governing equations, and allows exact specification of boundary conditions. The mathematics of this formulation is quite lengthy and involved and due to space limitations, only an outline is presented below. This paper summarizes these formulations. Future papers will cover application of this model to void geometry determined from real fractures.

Formulation

The Navier-Stokes' equations expressed in a coordinate-free form are given as follows:

$$\underset{\sim}{u} \cdot \underset{\sim}{\nabla} \underset{\sim}{u} = - \underset{\sim}{\nabla} p/\rho + \nu \nabla^2 \underset{\sim}{u} \tag{1}$$

Here, $\underset{\sim}{u}$ and p are the velocity vector and pressure respectively. ρ and ν are the fluid density and kinematic viscosity respectively. In three dimensions, there are three equations arising from Equation (1), one for each velocity component. Pressure is taken to be determined from the incompressibility constraint,

$$\underset{\sim}{\nabla} \cdot \underset{\sim}{u} = 0 \tag{2}$$

Equations (1) and (2) are solved subject to boundary conditions which include,

(a) no slip of fluid particles on solid surfaces,

(b) specified pressure at inlet and exit locations of flow and

(c) pressure gradient at fracture walls determined from the momentum equations (Equations 1).

When pressure is specified across a fracture, the amount of flow in it must be obtained as a solution of Equations (1) and (2). The flow boundary conditions can be prescribed as either periodic or a profile with an adjustable mean value. Results employing periodic boundary conditions are reported here, and this has the implication that the segment of geometry considered as a flow domain repeats indefinitely on both sides of the fracture where pressure is known.

The system of Equations (1) and (2) gives rise to one dimensionless parameter, the Reynolds number, $Re = UL/\nu$. U is the velocity scale $= \sqrt{\Delta p/\rho}$ and L is the length scale, typically the size of a contact area or the fracture aperture. With the scales properly defined, Reynolds number can be interpreted as the ratio of inertial to viscous forces. The magnitude of Re determines the choice of the numerical scheme which would be applicable to Equations (1) and (2). Fracture flows fall in the category of low Reynolds number flows, with viscous effects being present over the entire flow domain. This renders the classification of the mathematical problem as elliptic [Peyret and Taylor, 1983], and accordingly the computational procedure described below is an "elliptic flow solver". This restricts the scope of this work to physical problems which do not exhibit boundary-layers, unsteadiness and turbulence. However, in all calculations, the inertial terms are fully retained, so that the variation of fracture permeability on flow rate itself can be studied. A typical value of an upper limit for low Reynolds flow is suggested from fluid mechanics literature to be Re $\approx$ 100. For regional pressure gradients experienced in groundwater flow in a porous medium, one obtains Re $\leq$ 1. Since fractures have larger apertures and also local pressure gradients could be larger than regional values, it is appropriate to suggest that the range $1 \leq$ Re ≤ 25 be used in fracture hydrology studies.

The incompressibility condition given by Equation (2) is expected to determine pressure, but does not contain pressure explicitly. This can cause singularity in an iterative procedure of matrix inversion arising from a zero diagonal term. In the present work, Equation (2) has been replaced by the Poisson equation of pressure derivable from the momentum equations, and is given below.

$$\nabla^2 p = \rho\Big(\nu\nabla^2 D - \underset{\sim}{\nabla} \cdot (\underset{\sim}{u} \cdot \underset{\sim}{\nabla}\, \underset{\sim}{u})\Big) \qquad (3)$$

where D, the dilatation is $\underset{\sim}{\nabla} \cdot \underset{\sim}{u}$. The system of Equations (1) and (3) now solve for the flow and pressure field.

Since Equation (2) is not being solved, $D = \underset{\sim}{\nabla} \cdot \underset{\sim}{u}$ will not be zero in the intermediate calculations, until close to convergence. Hence D and terms containing D in Equation (3) must be determined and included in the iterative computations of the flow field.

Treatment of Geometry

In using a numerical method, it is most convenient when boundary conditions are imposed on constant coordinate surfaces. In this respect, a complex fracture geometry poses a problem.

The present work uses the idea of a natural coordinate system, which is illustrated in Figure 1. It is assumed that for every geometry which appears as irregular in the Cartesian (x-y-z) space, there exist coordinates (u-v-w), called as 'natural coordinates', which make it appear rectangular. A detailed discussion on coordinate systems which conform to the boundaries of the flow domain, and techniques of their generation are available elsewhere [Thompson, ed., 1982]. The flow calculation is performed in the regularized space using modified forms of Equations (1) and (3), which account for a change in the measure of distance, between the two coordinate systems. This step introduces severe complexity to the numerical procedure, since the Navier-Stokes' equations in generalized coordinates include a large number of mixed derivatives. For example, the Laplace operator, which has three terms in a three dimensional Cartesian space, requires 27 such terms to be fully expressible in a non-orthogonal coordinate system. This expanded form has to be applied to each of the three components of the velocity vector and pressure. This results in a computationally intensive computer code. However, the advantages of pursuing this direction are the simplification of geometry to one on which boundary-conditions can be exactly specified, and a uniform grid on which finite-difference rules can be easily applied.

The idea of transformation of coordinates has a major advantage in that finite difference methods based on Taylor's series expansion can be extended to cover problems involving complex geometries. There are other techniques such as the finite element method, which can incorporate variable geometry in the formulation and not require special treatment. There is no clear reason at this time to prefer one approach over the other. The finite element method, in particular, can generate large amounts of algebraic complexity, especially while solving three dimensional Navier-Stokes equations. The application of a pressure boundary condition on a no-slip wall is also known to be quite cumbersome, within the framework of finite elements. To this extent, the technique presented in this work retains the advantages of finite differences such as simplicity and easy application of pressure boundary conditions, while allowing the geometry to deviate from an orthogonal coordinate system.

The natural coordinates used for computation are derived in this work from a variational principle, which requires the distribution of the coordinate lines to be smooth and regular, with the constraint that their intersection with other coordinate lines be nearly orthogonal.

Numerical Solution

Equations governing grid generation and the flow respectively are coupled, non-linear, second order partial differential equations. They have been solved by finite-differences [Anderson et al., 1984]. This reduces the problem to one of matrix inversion which is performed by Gauss-Seidel iteration. For example, the equation,

$$\nabla_p^2 = Sp \quad ,$$

on a Cartesian grid can be approximated as,

$$\frac{(p_{i+1} + p_{i-1} - 2p_i)_{jk}}{(\Delta x)^2} + \frac{(p_{j+1} + p_{j-1} - 2p_j)_{ik}}{(\Delta y)^2} \tag{4}$$

$$+ \frac{(p_{k+1} + p_{k-1} - 2p_k)_{ij}}{(\Delta z)^2} = Sp_{ijk} \quad ,$$

and subsequently solved for p_{ijk}. This continues until convergence is observed. The unknown quantities in the grid generation equations are the locations of nodal points in the fracture, corresponding to a predetermined choice of grid in the natural coordinate system. For the flow problem, this is the velocity and pressure field. Each set of unknowns is simultaneously calculated at every grid point, before a new cycle of iteration begins. This continues until a prescribed convergence criterion (typically, 0.01 percent) is met. Complete solution of the grid equations is necessary before the flow field can be obtained.

The sequence of calculation of flow in a complex geometry can be summarized as follows.

(1) Choose appropriate computational space (CS) defined by the natural coordinates.

(2) Determine the equivalence between CS and the fracture by solving the coordinate generation equations.

(3) Solve flow equations in CS.

(4) Combine results of steps 2 and 3 to extract the flow solution in the fracture.

The non-linear inertial terms appearing in Equation (1) are approximated by a hybrid-upwind procedure, to ensure diagonal dominance for the convergence of the iteration scheme. This requires switching between a first and a second order finite-difference formula, based on the magnitude of the local Peclet number, Pe, [Patankar, 1980]. The scheme can be described as follows.

$$\frac{\partial}{\partial x}(u\phi) \approx \frac{u_e\phi_e - u_w\phi_w}{\Delta x} \tag{5}$$

where

$$
\begin{aligned}
u_e &= (u_{i+1} + u_i)/2 \\
u_w &= (u_{i-1} + u_i)/2 \\
\phi_e &= (\phi_{i+1} + \phi_i)/2 && \text{if } |\,Pe\,| < 2\,, \\
&= \phi_i && \text{if } Pe > 2\,, \\
&= \phi_{i+1} && \text{if } Pe < -2\,, \\
\phi_w &= (\phi_{i-1} + \phi_i)/2, && \text{if } |\,Pw\,| < 2 \\
&= \phi_i && \text{if } Pw > 2\,, \\
&= \phi_{i-1} && \text{if } Pw < -2\,.
\end{aligned}
$$

and

$$
\begin{aligned}
Pe &= u_e\, \Delta x/\nu \\
Pw &= u_w\, \Delta x/\nu\,.
\end{aligned}
$$

While dealing with a complex geometry, the Peclet number is defined in terms of the contravariant component of velocity. The use of the hybrid scheme reduces the accuracy of the overall numerical scheme formally to first order.

Results

Results given here are simple cases we have studied in the development of the model. Future papers will give the application of this model to the void geometry of real fractures. All calculations reported in this study employ a grid, whose discretization level is about 10 percent. Mass balance is estimated to be within 5 percent, and is seen to improve with grid refinement. The discrepancy in mass balance between inlet and outlet is exactly zero. For this reason error in mean velocity through a fracture is expected to be smaller than the maximum error in mass balance. The computer programs have been tested by reproducing exactly the flow pattern in a channel with parallel walls.

Figure 2 shows two views of a three dimensional duct with a square contact area located at its center. The side, top and bottom boundaries are closed and flow enters the left side and leaves on the right, in response to a pressure drop. Figure 3 shows a velocity vector plot at the mid-lane of the channel.. A roll pattern is clearly seem on the rear side of the obstruction. Structures of this type can be expected to impart non-linearity to the response of the flow system. Further, these can be simulated only if the complete flow equations are employed. The detailed calculation of the flow in the interior of the flow domain is expected to be the primary application of this technique. Figure 4 shows a plot of mean velocity as a function of Reynolds number for this duct with a contact area (marked 2), compared with a parallel channel (marked 1). The slope of the mean velocity curve is a measure of permeability of the fracture. On account of greater resistance to flow due to the contact area, curve 2 has a smaller slope than 1, everywhere. Curve 2 also exhibits mild non-linearity. This shows that at higher flow rates, the permeability is reduced further, because additional pressure drop is required to support the recirculation pattern visible in Figure 3.

Figure 5 shows a square region with a circular contact area. Since this flow domain is not describable in entirely Cartesian coordinates, the idea of natural coordinates is required. In the computational space, the obstacle is a square. Figure 5 also shows the equivalent coordinate lines in the two systems. Figure 6 shows a velocity vector plot of flow past the circular contact area at a Reynolds number of 5. The periodicity condition along with the smoother profile of a circle compared to a square eliminates the formation of a roll structure beyond the obstacle. Figure 7 shows a plot of mean velocity as a function of Re, for this case and can be seen to be linear. the comparable case of no obstacle is given by the equation

$$u_m = \frac{1}{2}\,\mathrm{Re} \quad , \tag{6}$$

for the dimensions assumed for the problem. The reduction in permeability (measured as a slope of the curve) is larger for this problem, since the contact area is itself larger, as compared to the case in Figure 2.

Figure 8 shows a channel with constrictions, along with its transformation into a parallel channel in terms of a generated coordinate system. Figure 9 shows the plot of mean velocity as a function of Re, for both a parallel channel and one with a constriction. Based on the cubic law, the slope of each line is proportional to the square of mean aperture. It is of interest to note that the equivalent aperture of the constricted channel is approximately 0.62, which is smaller than the smallest opening (0.7) in the wavy channel. This suggests that equivalent aperture calculations cannot be based on geometry alone and instead depend on flow dynamics contained within them.

References

Anderson, D. A., Tannehill, J. C. and Pletcher, R. H., 1984, *Computational Fluid Mechanics and Heat Transfer,* McGraw Hill, New York.

Hopkins, D., Cook, N. G. W., Myer, L. R., 1987, "Fracture Stiffness and Aperture as a Function of Applied Stress," to be presented at U. S. Rock Mechanics Symposium, Tucson, Arizona, 27-29 June, 1987.

Patankar, S. V., 1980, *Numerical Heat Transfer,* Hemisphere, Washington, D. C.

Peyret, R. and Taylor, T. D., 1983, *Computational Methods of Fluid Flow,* Springer Verlag, New York.

Pyrak-Nolte, L. J., Myer, L., Cook, N. G. W., and Witherspoon, P. A., 1987, "Hydraulic and Mechanical Properties of Natural Fractures in Low Permeability Rock", to be presented at 6th International Congress on Rock Mechanics, held in Montreal, Canada, 30 August, 1987.

Schlichting, H., 1979, *Boundary-Layer Theory,* McGraw Hill, New York.

Thompson, J. F., Editor, 1982, *Numerical Grid Generation,* Elsevier Science Publishing Company, New York.

Tsang, Y. W., 1984, "The Effect of Tortuosity on Fluid Flow through a Single Fracture", *Water Resources Research,* Vol. 20, pp. 1209-1215.

Nomenclature

D	Dilatation of flow, $= \underset{\sim}{\nabla} \cdot \underset{\sim}{u}$.
i,j,k	Column and row index on a finite difference grid.
L	Characteristic length, e.g., fracture opening.
p	Pressure.
Δp	Pressure drop across the fracture.
Pe	Peclet number.
Re	Reynolds number, $= UL/\nu$.
$\underset{\sim}{u}$	Velocity vector.
u,v,w	Natural coordinate system.
U	Characteristic velocity, $\sqrt{\frac{\Delta p}{\rho}}$.
u_m	Mean velocity through the fracture
x,y,z	Cartesian coordinate system.
$\Delta x, \Delta y, \Delta z$	Grid spacing in Cartesian space.
ρ	Fluid density.
ν	Kinematic viscosity.
$\underset{\sim}{\nabla}$	Gradient operator $(\frac{\partial}{\partial x}, \frac{\partial}{\partial y}, \frac{\partial}{\partial z})$.
ϕ	Generic variable

Figures

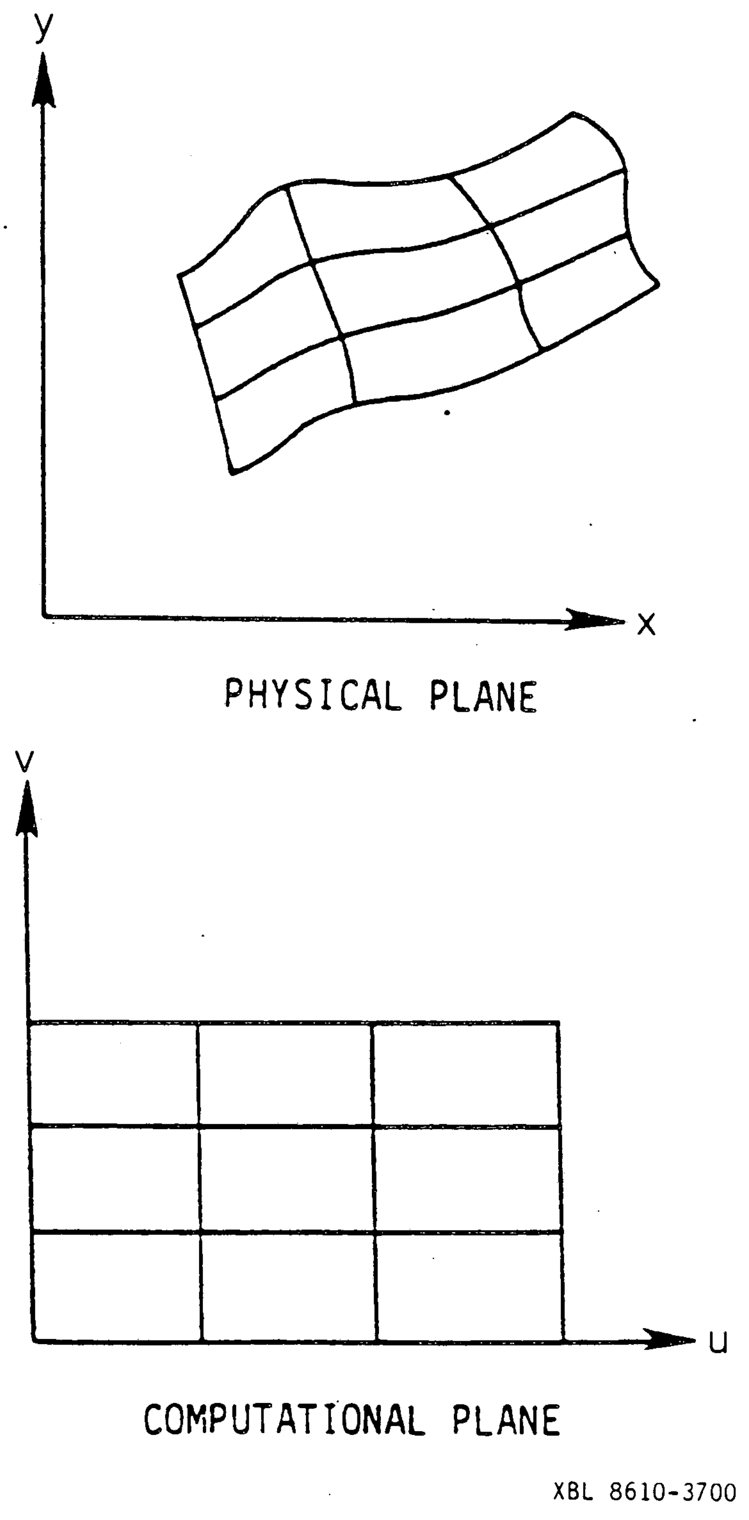

Fig. 1

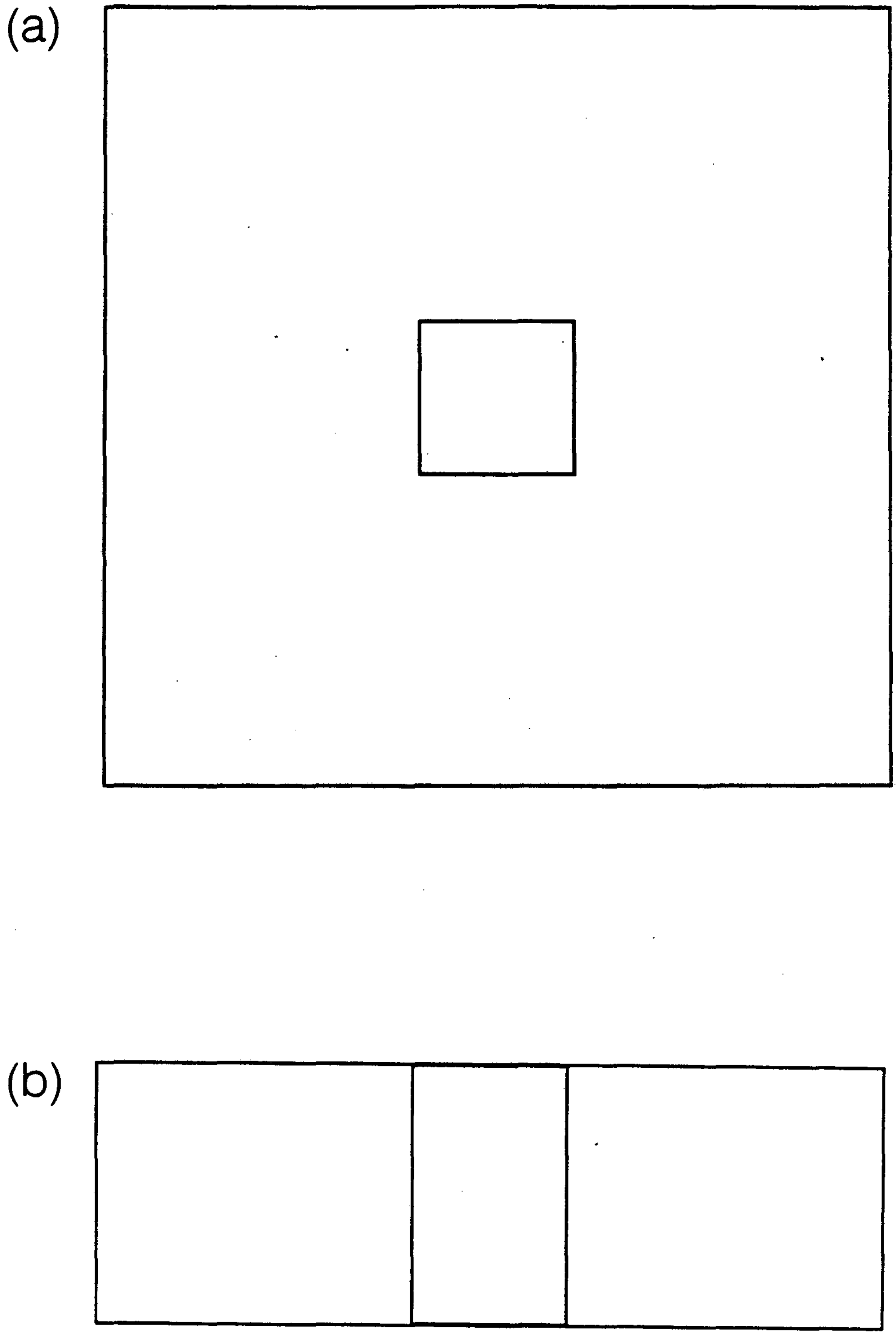

XBL 8610-3693

Fig. 2

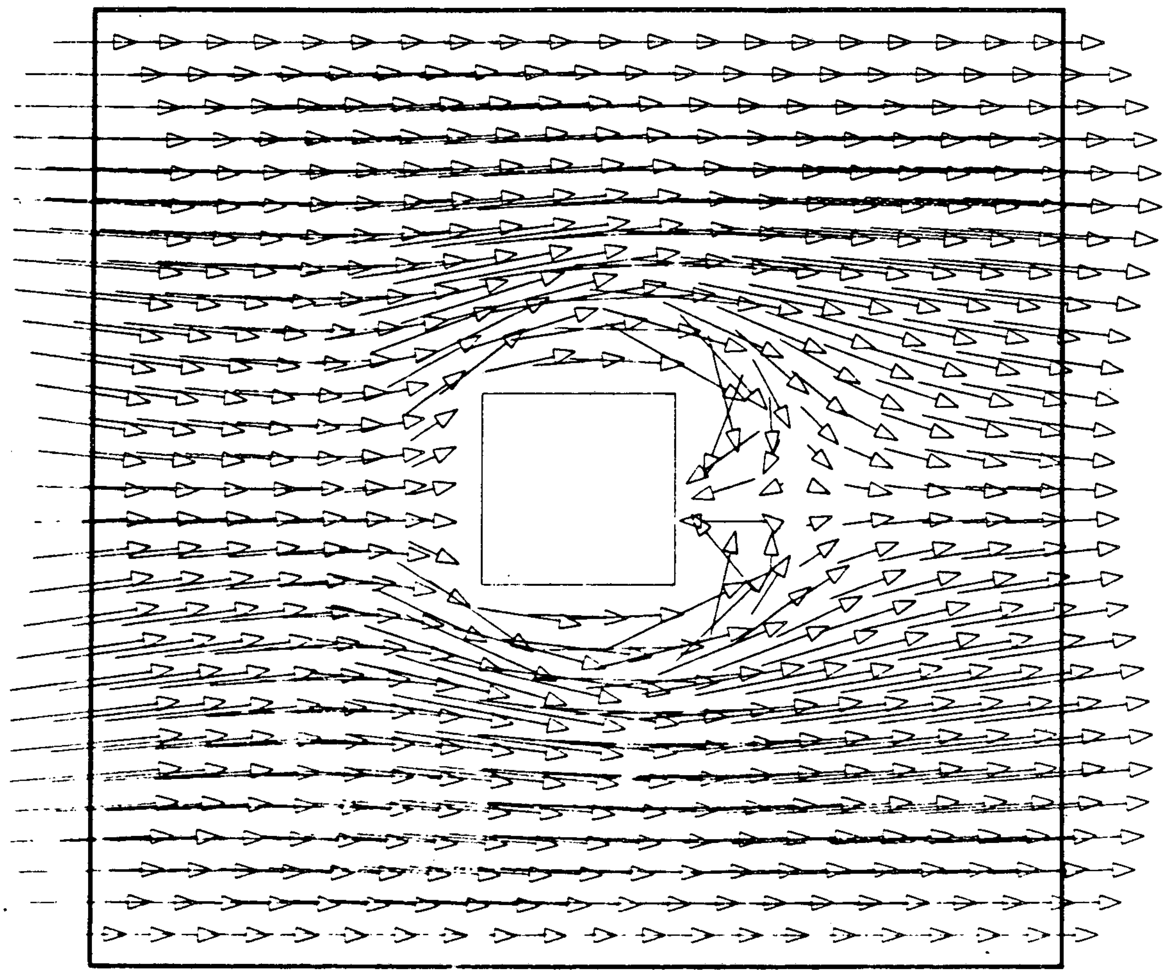

XBL 8610-3686

Fig. 3

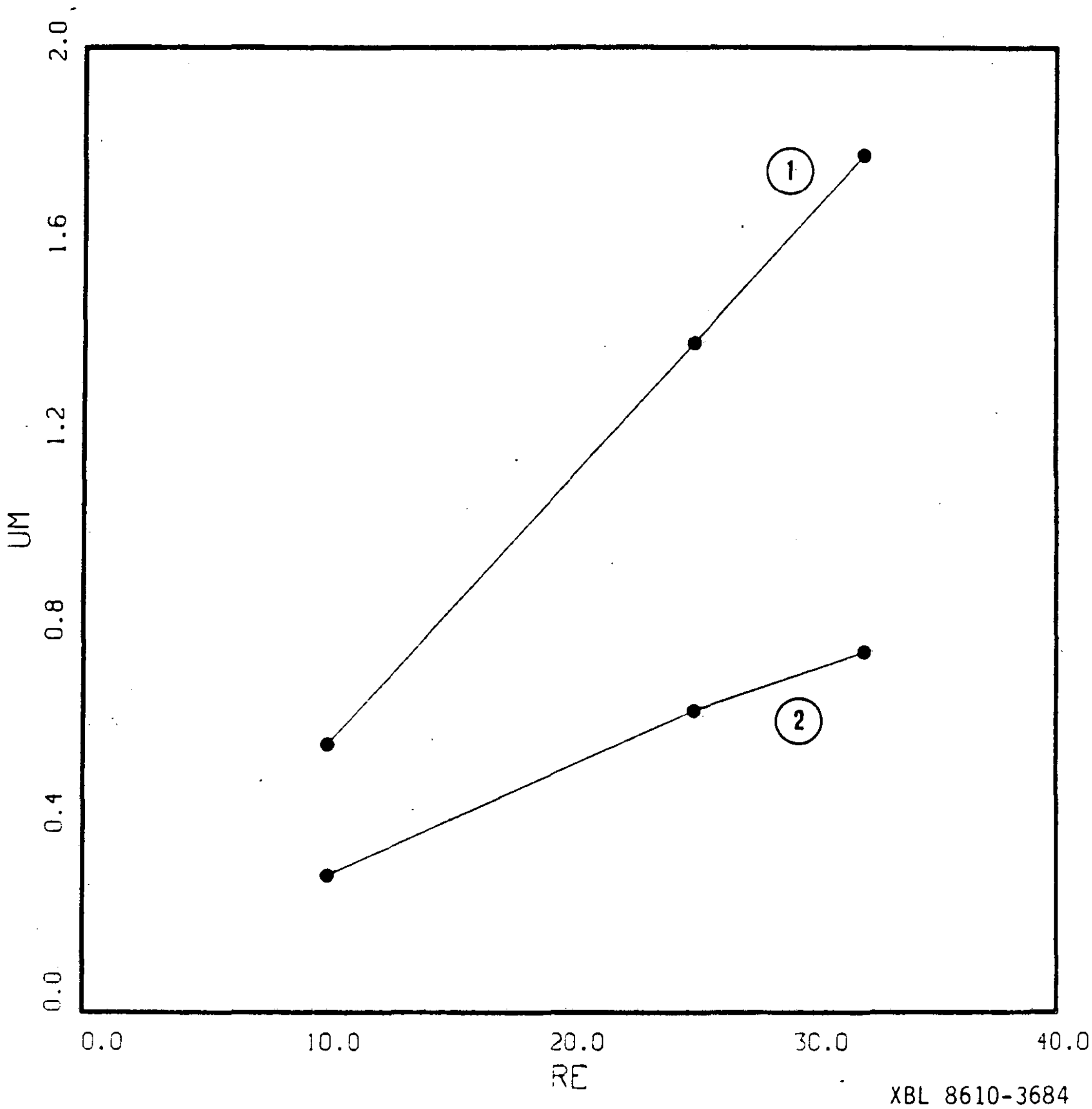

Fig. 4

(a)

(b)

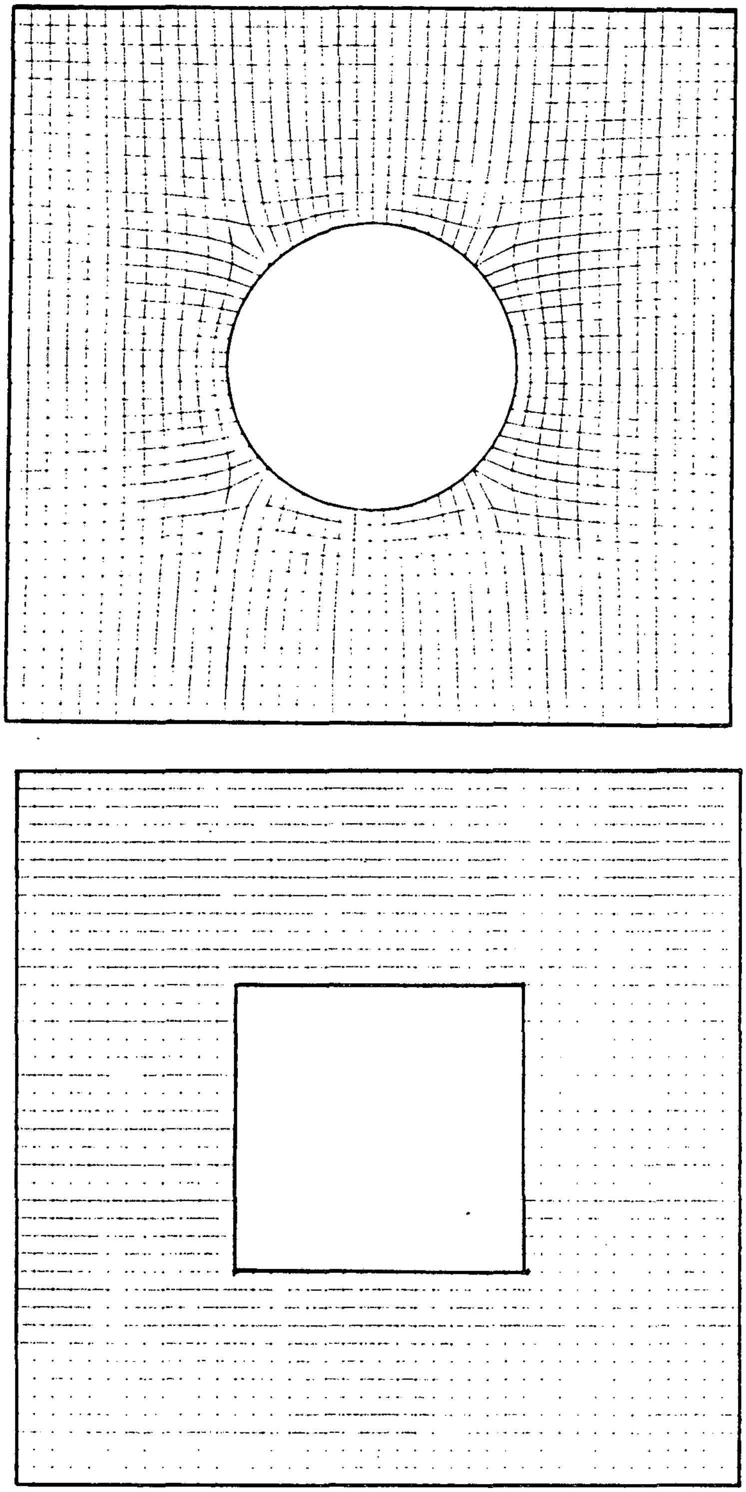

XBL 8610-3696

Fig. 5

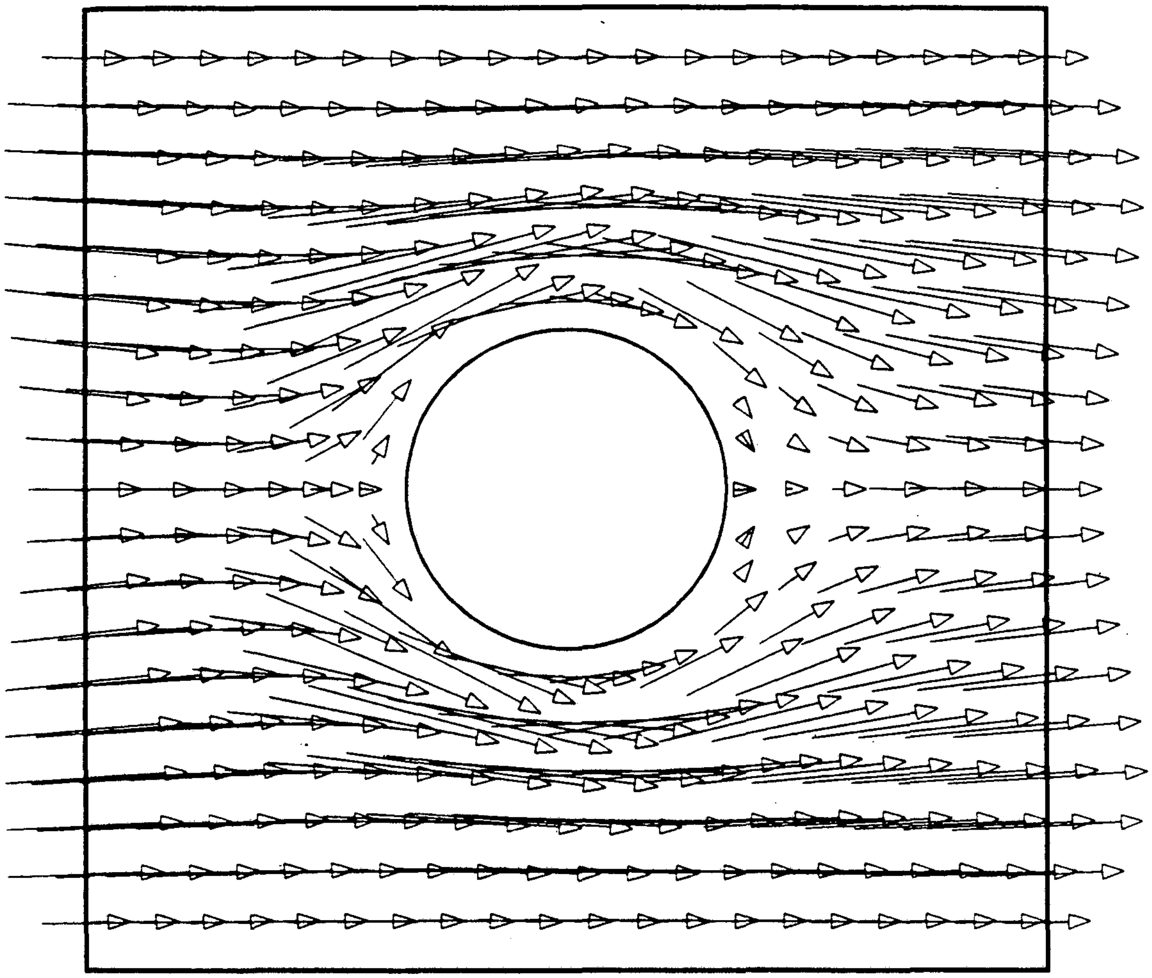

XBL 8612-4968

Fig. 6

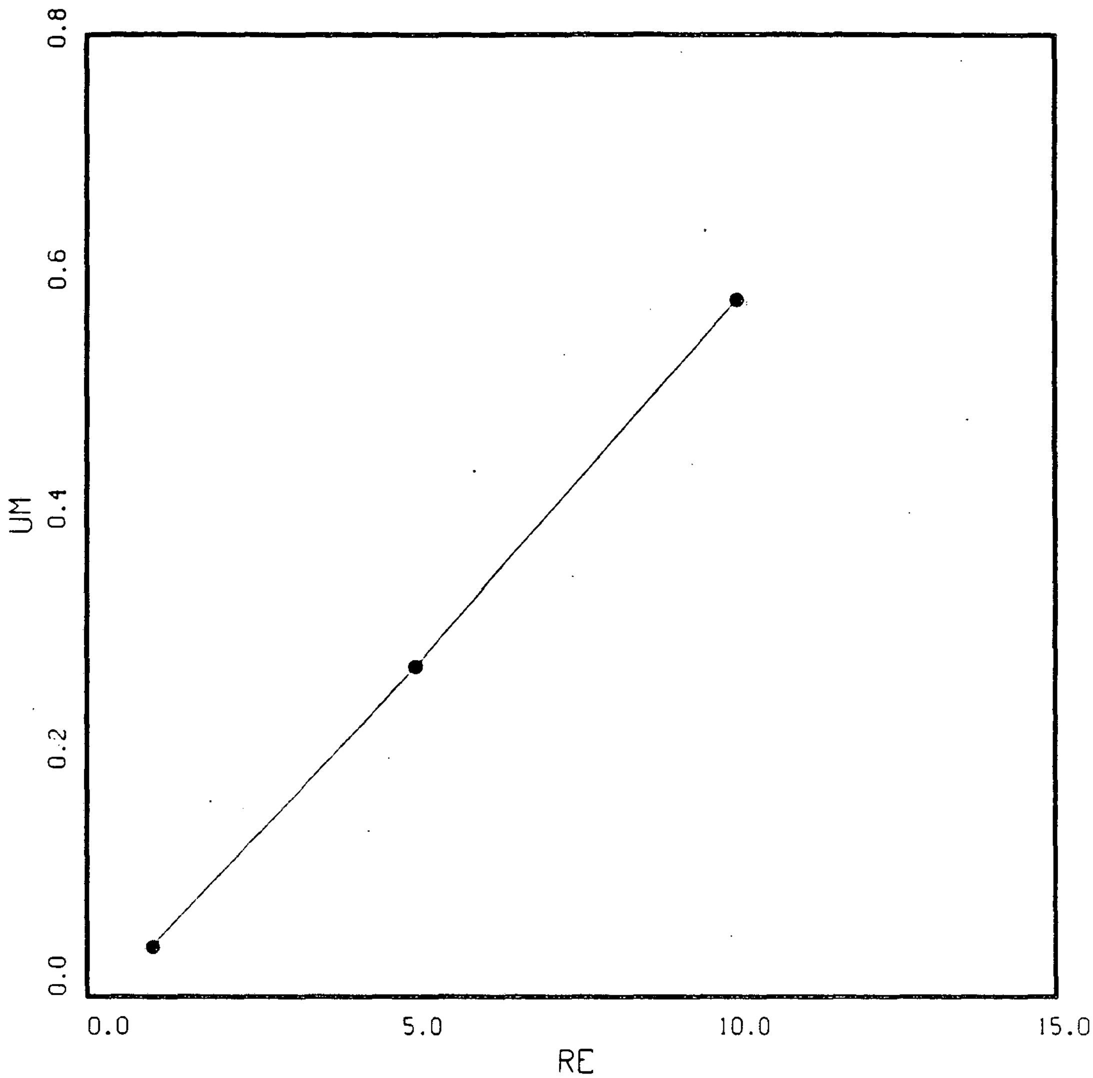

XBL 8612-4967

Fig. 7

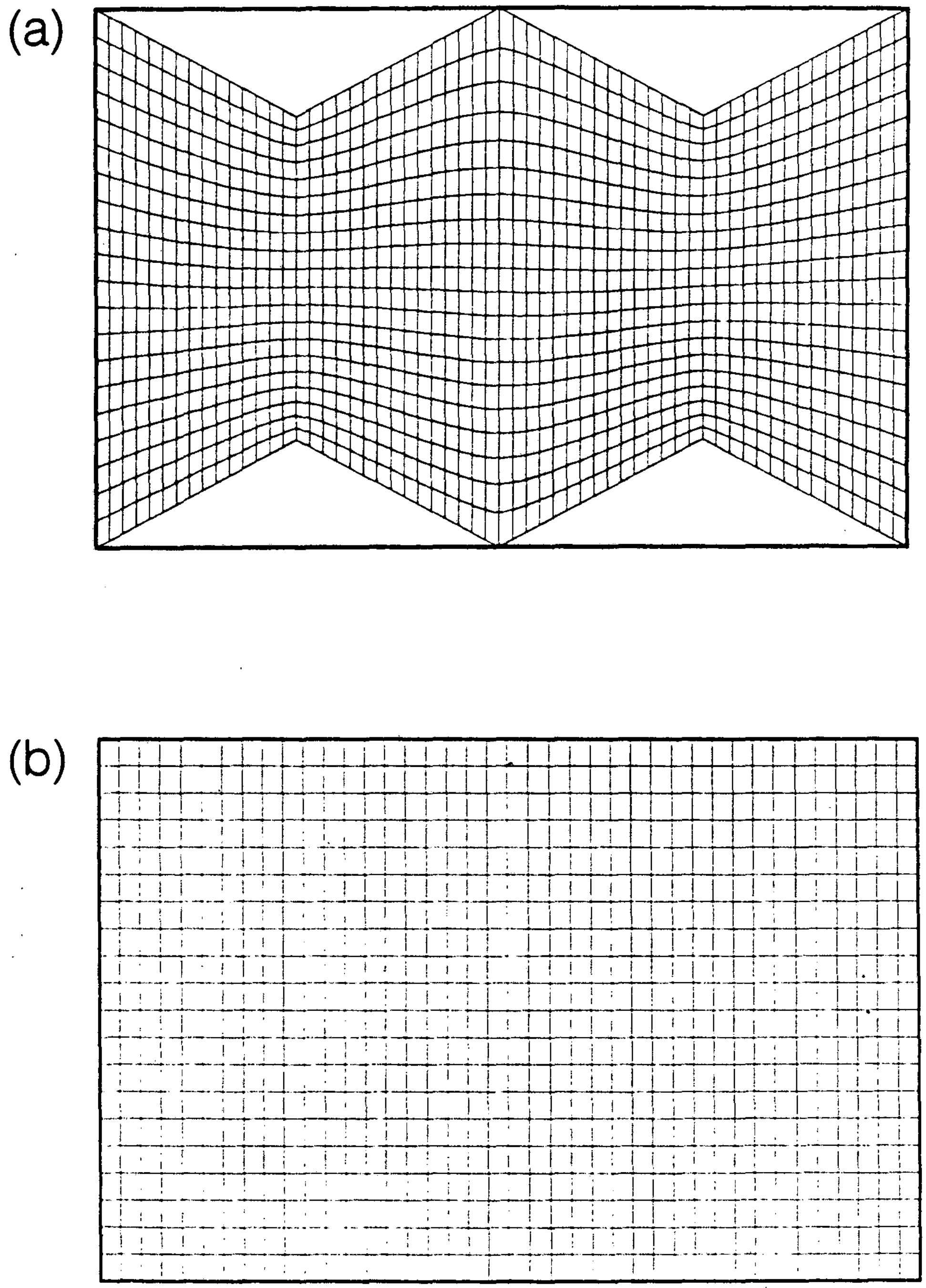

XBL 8610-3691

Fig. 8

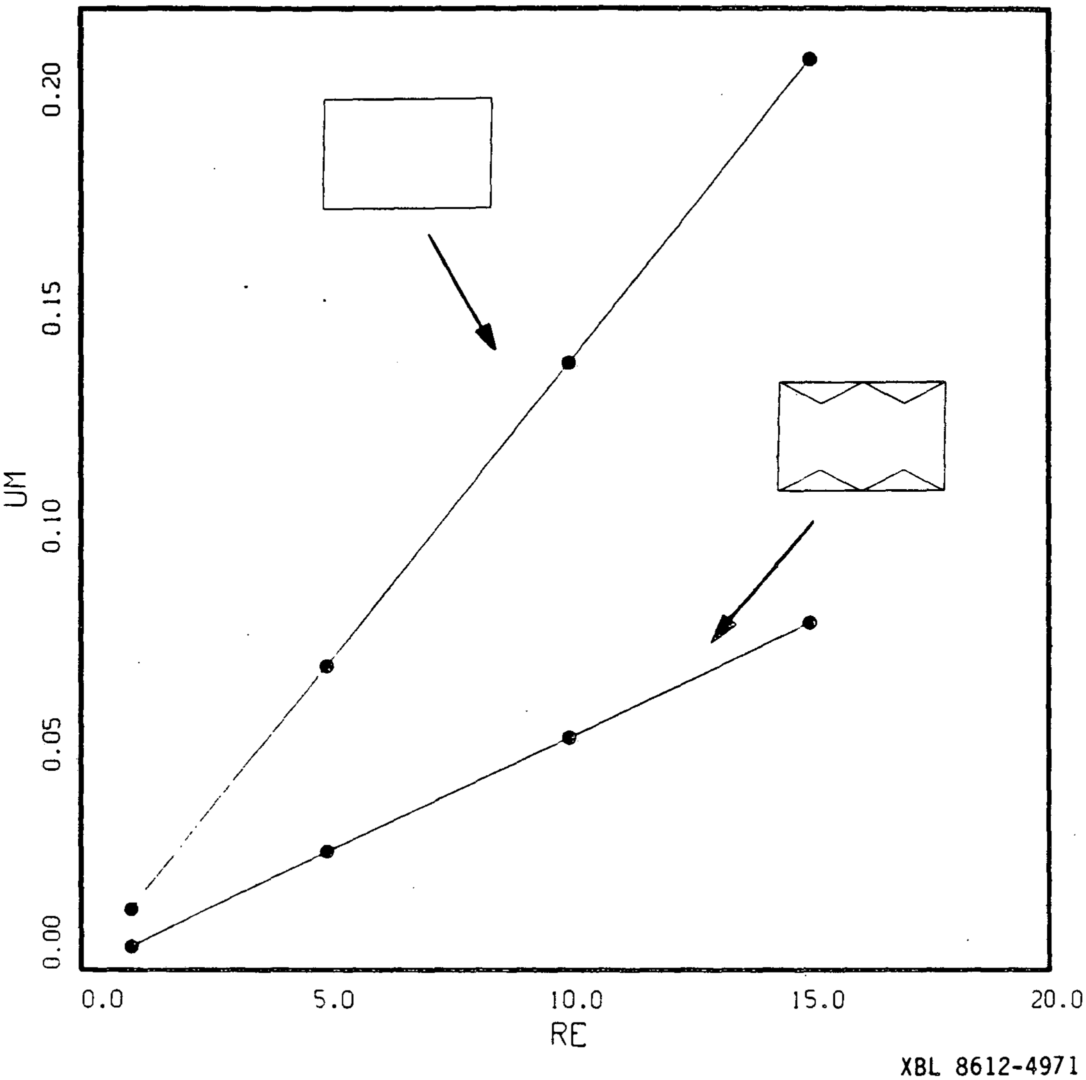

Fig. 9

LAWRENCE BERKELEY LABORATORY
TECHNICAL INFORMATION DEPARTMENT
UNIVERSITY OF CALIFORNIA
BERKELEY, CALIFORNIA 94720